www.sciencemag.org/cgi/content/full/337/6102/1668/DC1

Supplementary Materials for

Sedlin Controls the ER Export of Procollagen by Regulating the Sar1 Cycle

Rossella Venditti, Tiziana Scanu, Michele Santoro, Giuseppe Di Tullio, Alexander Spaar, Renato Gaibisso, Galina V. Beznoussenko, Alexander A. Mironov, Alexander Mironov Jr., Leopoldo Zelante, Maria Rosaria Piemontese, Notarangelo Angelo, Vivek Malhotra, Barbara M. Vertel, Cathal Wilson, Maria Antonietta De Matteis*

*To whom correspondence should be addressed. E-mail: dematteis@tigem.it

Published 28 September 2012, *Science* **337**, 1668 (2012)
DOI: 10.1126/science.1224947

This PDF file includes:

Materials and Methods

Reagents and antibodies

All chemical reagents were of analytical grade or higher and purchased from Sigma (St Louis, MO) unless otherwise specified. Sedlin, Bet3 (TRAPPC3) and Synbindin (TRAPPC4) polyclonal antibodies for immunoblotting and immunofluorescence were raised in rabbits by immunization with recombinant glutathione S-transferase (GST)-fusion full-length proteins. The antibodies were affinity purified over columns conjugated with a His fusion of the respective protein. Polyclonal antibodies against GRASP55, Sec31, GST, GM130 and mAb CD8 were produced similarly, as described previously (*21, 22*). Other antibodies used in this study were from the following sources: mAb GM130 (BD Biosciences), β-actin (Sigma) and His (Qiagen), GAPDH (Santa Cruz), PC-I SP1D8 and PC-II (Hybridoma Bank), VSV-G P5D4 (Bethyl Laboratories), PC-I HC-I (Daichii Pure Chemicals), TGN46 and TGN38 (Serotech), albumin and α1-antitrypsin (Dako Cytomation), Sec23 (ABR Affinity BioReagents), Sar1 (Upstate Biotechnology), mAb anti-active Sar1 (NewEast Bioscience). Alexa-conjugated secondary antibodies were from Invitrogen, while HRP-conjugated secondary antibodies were purchased from Calbiochem.

Cloning/Vectors

cDNAs encoding wild type hSedlin and the R90X mutant were a kind gift of the Gécz lab. The H13A and del387a mutations in human Sedlin were generated using the Quickchange mutagenesis system (Agilent Technologies) following the manufacturer's protocol. hBet3 and hTrs31 cDNA were purchased from imaGenes GmbH (IMAGE number 3051295 and 4869377, respectively) and inserted into the pGEX-4T plasmid. The CD8 cDNA was kindly provided by Professor Stefano Bonatti. The full-length hSec23A coding sequence was subcloned from the pFAST-BAC-DUAL hSec23A-Sec24D plasmid kindly provided by William Balch and inserted into the BglII/XhoI sites of the vector pEGFP-C2 and in pET28A (Clontech Laboratories). The pGEX4T hSar1A was kindly provided by Randy Schekman. The h Sar1B WT and Sar1B H79H coding sequences were subcloned from the pET11d –h Sar1B WT and Sar1B H79H plasmids kindly provided by William Balch and inserted into the pET-28a, p-GEX-4T and pEGFP-C plasmids. To generate fluorescent tagged PC II, the cDNA sequence corresponding to amino acids 26-1487 of COL2A1 was PCR-amplified from the Image clone IRCFp5008C071D (imaGenes GmbH) using the forward primer 5'-TTCAAGCTTGTCAGGATGTCCAGGAGGCTG-3' and reverse primer 5'-GAGGGATCCTTACAAGAAGCAGACCGGCC-3' and cloned HindIII/BamHI into the pmCHERRY-C2 vector, a derivative of pEGFP-C2. This construct was digested with NheI/AgeI and a stuffer fragment corresponding to the procollagen signal peptide (amino acids 1-25) that included the Kozak consensus sequence was ligated upstream of the mCHERRY by annealing the oligos 5'-CTAGCACCATGGCAATTCGCCTCGGGGCTCCCCAGACGCTGGTGCTGCTGAC GCTGCTCGTCGCCGCTGTCCTTCGGTGTCAGGGCA-3' and 5'-CCGGTGCCCTGACACCGAAGGACAGCGGCGACGAGCAGCGTCAGCAGCACC AGCGTCTGGGGAGCCCCGAGGCGAATTGCCATGGTG-3'.

Cell Culture

Human fibroblasts, HeLa cells and Rx chondrocytes (*23*) were grown in high glucose (4500 mg/L) DMEM supplemented with 2 mM L-glutamine (containing sodium pyruvate for the Rx chondrocytes), primary fibroblasts in RPMI supplemented with 2 mM L-glutamine, and HepG2 cells in MEM supplemented with 1% non-essential amino acids. All media contained 50 IU/ml penicillin, 50 µg/ml streptomycin and 10% foetal calf serum (FCS). Cells were grown at 37°C in 5% CO_2 and at 98% humidity. Media, serum and reagents for tissue culture were purchased from GIBCO™ (Invitrogen).

siRNA treatments

siRNA sequences used in this study are listed in Table S1. Rx chondrocytes, NRK fibroblasts, HepG2 cells and HeLa cells were treated for 72 h with Sedlin, TANGO1 or Bet3 siRNAs. Human fibroblasts were treated for 96 h with Sedlin siRNA or for 72 h with Bet3 siRNA using electroporation.

Sedlin depletion: as Sedlin is encoded by two different genes (the gene on chromosome X whose mutation is responsible for SEDT and an "active" pseudogene on chromosome 19) (*24*), Sedlin KD was performed using a smart-pool of four Sedlin siRNAs from Dharmacon (N1-N4, used for all experiments) directed against both genes. The effects of the N1-N4 smart-pool, which reduced Sedlin levels to 15% of control values, were compared with a pool of two overlapping siRNAs (S1-S2, corresponding to the ones used in ref. *12*), which induced a reduction of the levels of Sedlin to 5% of control values (Fig. S4A). A possible reason for the higher efficacy of the S1-S2 Sedlin siRNAs may be the fact that they also target the Sedlin-processed pseudogene on chromosome 8 (*24*), and that processed pseudogenes may control the stability of mRNAs transcribed from active genes (*25*). The levels of Sedlin depletion using the N1-N4 pool that impaired the exit of PC from the ER did not affect organization of the Golgi complex as assessed by EM analysis and immunofluorescence (Fig. S2 and S4). However, the Golgi complex appeared fragmented when HeLa cells were treated with the Sedlin S1-S2 pool. Thus, under the experimental conditions used for Sedlin depletion with the N1-N4 siRNAs, residual levels of Sedlin (15% of control value) limit the ER-export of PC but remain permissive for the maintenance of the Golgi complex, highlighting a sharp dependence of the ER export of PC on normal Sedlin levels. Indeed, these KD conditions perfectly mimic those of cells from SEDT patients where the ER export of PC is defective (Fig. 1G) while the function and structure of the Golgi complex are preserved (Fig.1G and Fig. S6B) (*6*), and where residual levels of wild type Sedlin may persist as a product of the transcribed retropseudogene on chromosome 19 (*6, 12*).

Bet3/TRAPP depletion: depletion of the entire complex was achieved by siRNA KD of the expression of the TRAPP subunit Bet3, which induces destabilization and possibly degradation of the entire complex (Fig. S1A) (*12*). As with Sedlin depletion, the exit of PCII and PCI, but not that of other cargoes (α1-antitrypsin, albumin, VSV-G and CD8α), from the ER was retarded (Fig. S3). However, in contrast to what was observed for Sedlin depletion, and in agreement with earlier reports (*26*) these cargoes were inhibited in a post-ER station in their transport to the PM (Fig. S3). This delay might be a consequence of the impact of TRAPP depletion on the structure of the Golgi complex that, as already reported (*26*), appeared extensively fragmented (Fig. S4B).

Acute TRAPP block

The acute block of TRAPP was achieved by microinjecting a blocking anti-Bet3 antibody. The acute block of TRAPP induced a more pronounced and persistent inhibition of the ER exit of PCII compared to the TRAPP depletion achieved through siRNAs (Fig. S5, A and B) and the Golgi complex was more markedly fragmented (Fig. S5). Similarly to TRAPP depletion by Bet3 KD, VSV-G transport out of the ER was not impaired (Fig. S5, C and D) but, as earlier reported (*26*), it was retarded in post-ER vesicular compartments (Fig. S5C, inset).

Transport assays

For VSV-G assays, cells were infected with the ts045-VSV variant for 1 hr at 32°C in serum-free medium. After infection, cells were washed several times and shifted for 3 hrs to 40°C in complete medium. Cycloheximide was added to a final concentration of 100 μg/ml and cells were shifted to 32°C for the indicated times. To follow endogenous PC-I in fibroblasts or PC-II in Rx chondrocytes (both endogenous and expressed in primary fibroblasts), cells were incubated for 3 hrs at 40°C in DMEM supplemented with 1% serum and 20 mM HEPES pH 7.2, then shifted to 32°C in the presence of cycloheximide (100 μg/ml) and ascorbate (50 μg/ml). Cells were then fixed and processed for immunofluorescence. Quantitative evaluation of VSV-G and PC (both I and II) transport was performed by analyzing the immunofluorescence staining patterns of at least 200 cells in three separate experiments.

For CD8α transport, cell nuclei were injected with CD8α cDNA, incubated 6 hrs at 37°C and then chased in the presence of cycloheximide (100 μg/ml) for the indicated times. Cells were fixed and processed for immunofluorescence.

Metabolic labeling

Total secretion experiments were performed essentially as described previously (*2*). For PCII secretion, CTRL or Sedlin KD chondrocytes were pulsed with ^{35}S-methionine for 60 min, then washed and chased. After 1, 2 and 3 hrs the medium and the cell lysates were immunoprecipitated with the anti-PCII specific monoclonal Ab, and the immunoprecipitates analyzed by SDS-PAGE followed by autoradiography. For albumin and α1-antitrypsin secretion, experiments were performed as previously described (*27*).

Clinical and genetic diagnosis of SEDT patients

Four related Italian patients were diagnosed as SEDT on the basis of a large pedigree suggestive of an X-linked mode of inheritance and clinical signs (short trunk, sternal protrusion, hip dysplasia and back pain) in combination with radiological findings. The symptoms were evident in late childhood. Informed consent was obtained from all individuals. Genomic DNA was prepared from blood lymphocytes by standard procedures.

Mutational analysis of the SEDL gene: Coding exons 3-6 (including exon/intron boundaries) of the SEDL gene were amplified by PCR under standard conditions using previously described primers for genomic PCR amplification and sequencing (*6*). PCR products were purified using an ExoSAP IT Kit (USB Corporation, GE Healthcare) and sequenced using a Big Dye Terminator ready reaction Kit (PE Applied Biosystems, CA, USA), according to the manufacturer's specifications, on an ABI PRISM 3100 Genetic

Analyzer (Applied Biosystems). The mutational analysis showed a hitherto undescribed mutation, c.387delA (p.K129fsX109), in the sixth exon of the SEDL gene. This deletion causes a frameshift and a premature stop codon, resulting in a truncated form of Sedlin (138 aa) with the first 129 aa identical to the wild type Sedlin and the remaining 9 C-terminal putative residues divergent because of the translational frameshift (Fig. S6A).
Primary fibroblast cultures: cutaneous specimens were placed in RPMI 1640 medium without serum immediately after biopsy removal, repeatedly washed with PBS and placed in a 30 mm Petri dish. The specimens were then fragmented in 1-2 mm pieces and transferred to flasks containing D-MEM (Invitrogen) supplemented with 10% Fetal Bovine Serum (FBS, Invitrogen), 100 units/ml penicillin and 100 µg/ml streptomycin. Primary cultures were incubated at 37°C in 5% CO_2 humidified atmosphere, and 5 ml of complete medium were added 24 hours later. After one week primary cultures were washed with PBS to remove non-adherent fragments and fresh medium prewarmed at 37°C was added. These procedures were repeated every 3 days until primary cultures reached local confluence.

FRAP and FLIP of GFP-Sec23

Human fibroblasts microinjected with a plasmid encoding GFP-Sec23 were incubated at 37°C in carbonate-free culture medium in a humidified temperature-controlled incubation chamber on a LSM710 confocal microscope (Zeiss) and imaged using a 488 nm argon laser and a 63x PlanApochromat NA 1.4 DIC oil immersion objective. FRAP and FLIP experiments and time-lapse laser-scanning confocal microscopy were performed as described (*28, 29*). The half time for recovery, $t_{1/2}$, and the dissociation constant (k_{off}) of GFP-Sec23 were calculated as previously described (*28, 30*).

Assay for Sar1 membrane association in permeabilized cells

HeLa cells treated with non-targeting, Sedlin or Bet3 siRNAs for 72 hrs were permeabilized with streptolysine-O (SLO) as previously described (*31*). The cytosolic and membrane-bound fractions were probed by immunoblot analysis using antibodies against Sar1, Sec23, Sec31, and GAPDH (as a control of permeabilization).

Validation of the anti-active Sar1 Antibody

We validated the ability of the anti-active Sar1 Ab from NewEast Bioscience to specifically recognize the GTP-bound form of Sar1 (Fig. S8). Following the manufacturer's instructions for cell lysis and immunoprecipitation, we verified that the Ab immunoprecipitates Sar1 from cell extracts only when Sar1 is loaded with GTP (and not with GDP) and it very effectively stains the GTP-locked form of Sar1 (Sar1H79G) in immunofluorescence while it does not stain the GDP-locked form (Sar1T39N) and recognizes only a subfraction of WT Sar1.

Recombinant Proteins

Recombinant GST-tagged proteins (hSedlin, hBet3, hTrs31, hSar1A and hSar1B) were expressed in BL21 E. coli from the pGEX-4T plasmid and purified using the Bulk GST purification module (Amersham Pharmacia Biotech) according to the manufacturer's instructions. GST was removed from Sar1A and Sar1B by thrombin digestion and the proteins purified according to the manufacturer's instructions (GE Healthcare). His-

tagged proteins (hSar1B, and the cytosolic domain of hTANGO1, 1211-1908 aa) were expressed in E. coli from pet28a-Sar1 WT or pet28a-Sar1H79G and purified according to the manufacturer's instructions (Qiagen, Ni-NTA agarose beads).

Pull-down assays

Increasing concentrations (0.1, 0.3 and 1 μM) of His-Sar1 were incubated with GST-fusion proteins or GST alone (0.5 μM) as previously described (*19*). After overnight incubation at 4°C in 300 μl binding buffer (50 mM TRIS pH 7.4, 100 mM NaCl, 1mg/ml BSA, 0.1% Triton X-100, 0.1% NP-40, 0.1 mM GTP or GDP), glutathione-beads were added, incubated for 2 hrs at 4°C, washed 5 times (50 mM TRIS pH 7.4, 100 mM NaCl), eluted and analyzed by SDS-PAGE.

Microscopy

Immunofluorescence microscopy was performed as described (*32*). Electron Microscopy and Tomography: Thick (150-200 nm) epon sections were cut with a Leica Ultracut-UCT microtome (Leica, Germany) and transferred onto formvar-coated copper slot grids. Sections were post-stained with Reynold's lead citrate. Colloidal gold particles (10 nm) were deposited on both surfaces of the sections and used as markers during the subsequent alignment of the series of tilted images. Specimens were analysed with a Tecnai 12 EM (FEI, The Netherlands) operating at 120 keV. The samples were tilted from +70° to –70° at 1° intervals, with magnification of 43,000X. The specimens were irradiated for 3 min with the electron beam before initiating the acquisition of the tilt series in order to limit anisotropic specimen thinning during data collection. The focus was regulated for each acquired image. The computer program IMOD 2.5.0 was then used to align the tilt series and to calculate the tomography reconstruction from the aligned tilt series. Surfaces of ER membranes and ERES were rendered using the IMOD software.

Computational modeling of the Sar1A-GTP:Sedlin complex

The coordinates of the SRβ-GTP:SRX complex, Sar1A-GTP, and Sedlin were taken from the Protein Data Bank (PDB entries 2FH5, 1M2O, and 2J3W, respectively). Missing residues were added using the SWISS MODEL (*33*). This software was also used for the superposition of Sar1A-GTP and Sedlin onto the SRβ-GTP:SRX complex. In silico docking experiments were performed using PatchDock and then further refined and ranked with FireDock. Molecular visualization and general analysis were done using the program Visual Molecular Dynamics (VMD).

Figure S1

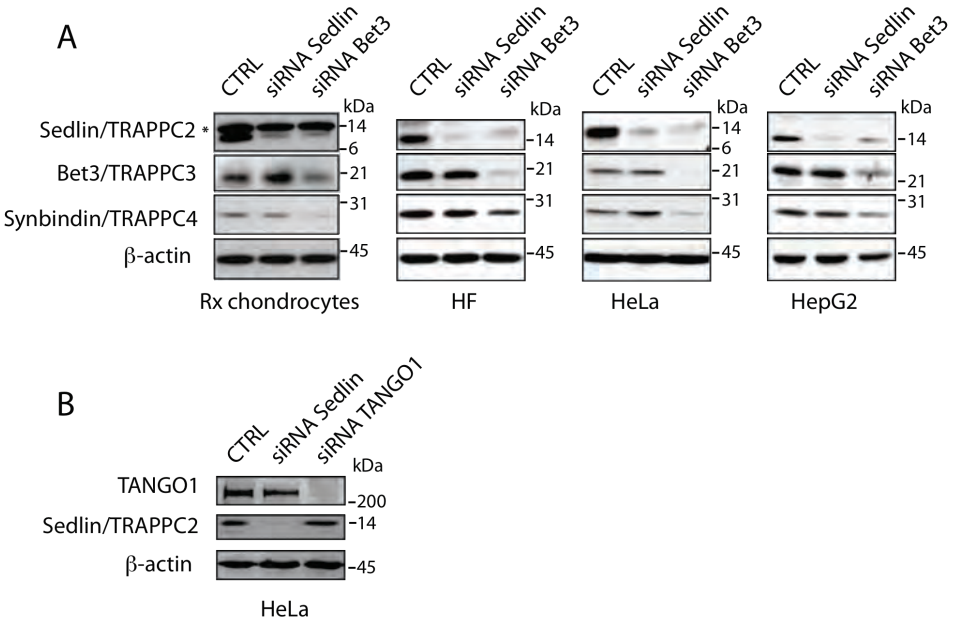

Fig. S1. siRNA treatments.

(A) Rx chondrocytes, human fibroblasts (HF), HeLa cells or HepG2 cells were treated with the indicated siRNA (see Table S1 and Materials and Methods). Cell lysates (60 μg/sample) were analyzed by SDS-PAGE and immunoblotting with the indicated antibodies. β-actin was used as a loading control. The asterisk indicates a non-specific band detected by the anti-Sedlin Ab in Rx chondrocytes. Notice that while Sedlin depletion does not affect the levels of the other TRAPP components analyzed, Bet3 depletion induces a decrease in the levels of the other TRAPP components analyzed possibly due to a destabilization of the entire TRAPP complex. These differential effects are in agreement with previous reports (*12*) and are likely to be due to the different positioning of Sedlin and Bet3 in the TRAPP complex, Sedlin being a peripheral and Bet3 a core component of TRAPP (*34*). **(B)** HeLa cells were treated with Sedlin or TANGO1 siRNA (see Table S1 and Materials and Methods). Cell lysates (60 μg/sample) were analyzed by SDS-PAGE and immunoblotting with anti-Sedlin and anti-TANGO1 antibodies. Notice that Sedlin depletion does not affect TANGO1 levels and vice-versa.

Figure S2

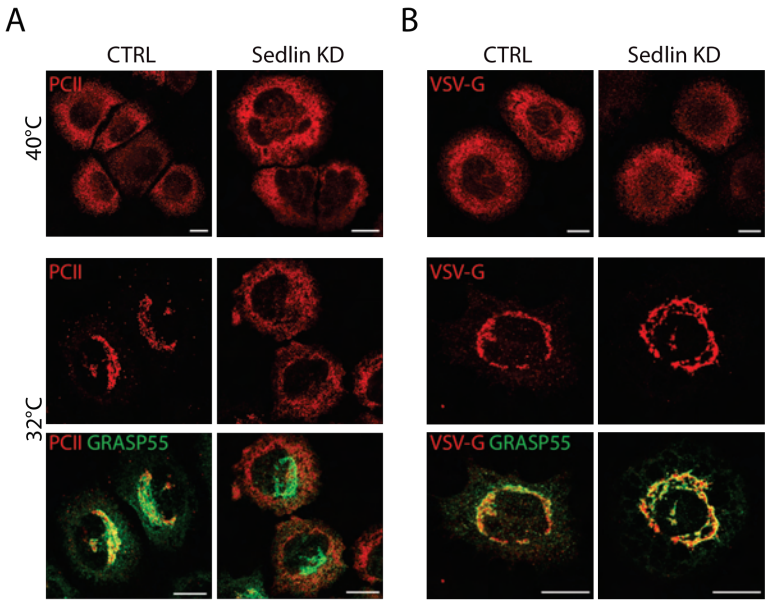

Fig. S2. Sedlin is selectively required for the ER exit of PC.
(A) PCII trafficking in Rx chondrocytes mock-treated (CTRL) or Sedlin siRNA-treated (Sedlin KD) and incubated for 3 hrs at 40°C (40°C), and then shifted to 32°C for 30 min (32°C), double stained with Ab against PCII (red) and against GRASP55 (a marker of the Golgi complex, green). Scale bars, 10 μm. **(B)** CTRL or Sedlin KD chondrocytes were infected for 1 hr at 32°C with ts045-VSV, then incubated for 3 hrs at 40°C (40°C) and afterwards shifted to 32°C for 30 min. VSV-G (red) and GRASP55 (green) were localized using specific antibodies. Scale bars, 10 μm.

Figure S3

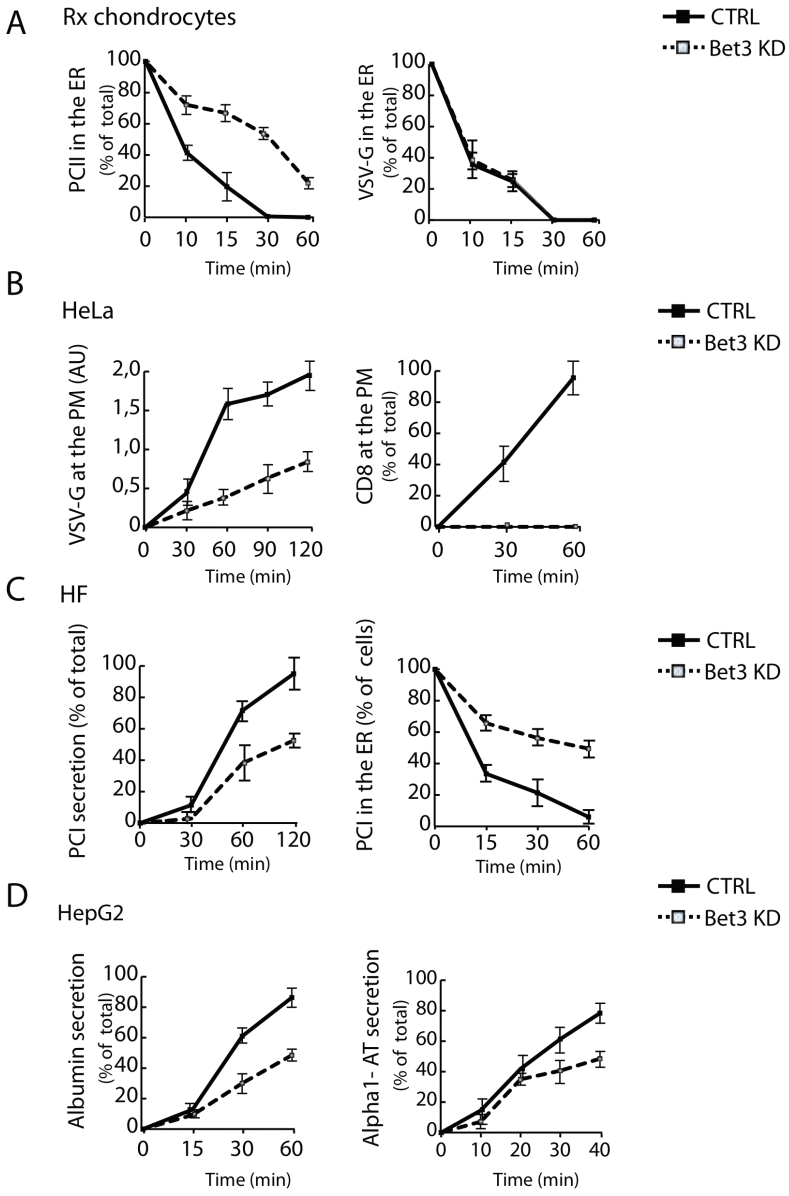

Fig. S3. The TRAPP complex is selectively required for the ER exit of PC.
Impact of depletion of the entire TRAPP complex, by siRNA of Bet3 (see Fig. S1), on the transport of **(A)** PCII and VSV-G in chondrocytes, **(B)** VSV-G and CD8α in HeLa cells, **(C)** PCI in human fibroblasts or **(D)** albumin and α1 anti-trypsin (Alpha1-AT) in HepG2 cells. The exit of PC, but not that of VSV-G, from the ER was retarded, while transport of all cargoes to the PM was inhibited. N=4.

Figure S4

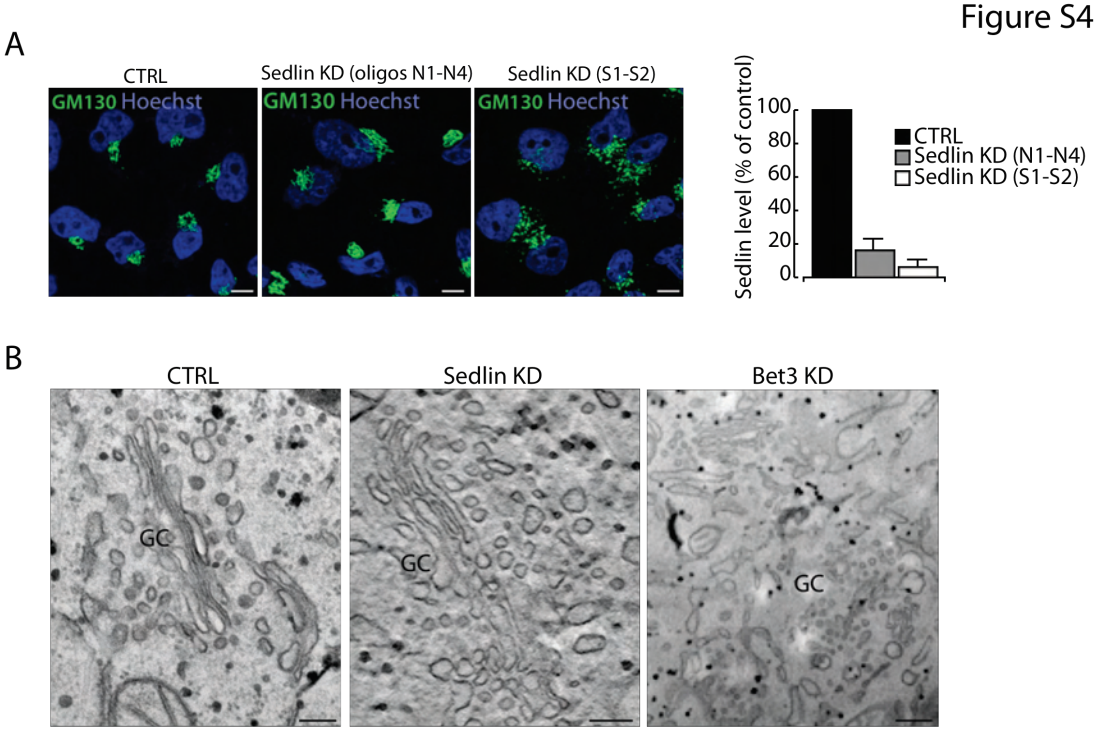

Fig. S4. Effect of Sedlin and of TRAPP depletion on the Golgi complex architecture.

(A) HeLa cells were treated with non-targeting (CTRL), Sedlin siRNAs N1-N4 or Sedlin siRNAs S1-S2 (Table S1, *12*), processed for IF and stained with anti-GM130 (green, as a Golgi marker) or with Hoechst 33258 (blue, as nuclear staining). Note that the two sets of siRNAs induce different levels of Sedlin depletion (right panel) and differentially affect the organization of the Golgi complex (left panels). See Materials and Methods for discussion. **(B)** HeLa cells were treated with non-targeting (CTRL), Bet3, or Sedlin (N1-N4) siRNAs and processed for EM.

Figure S5

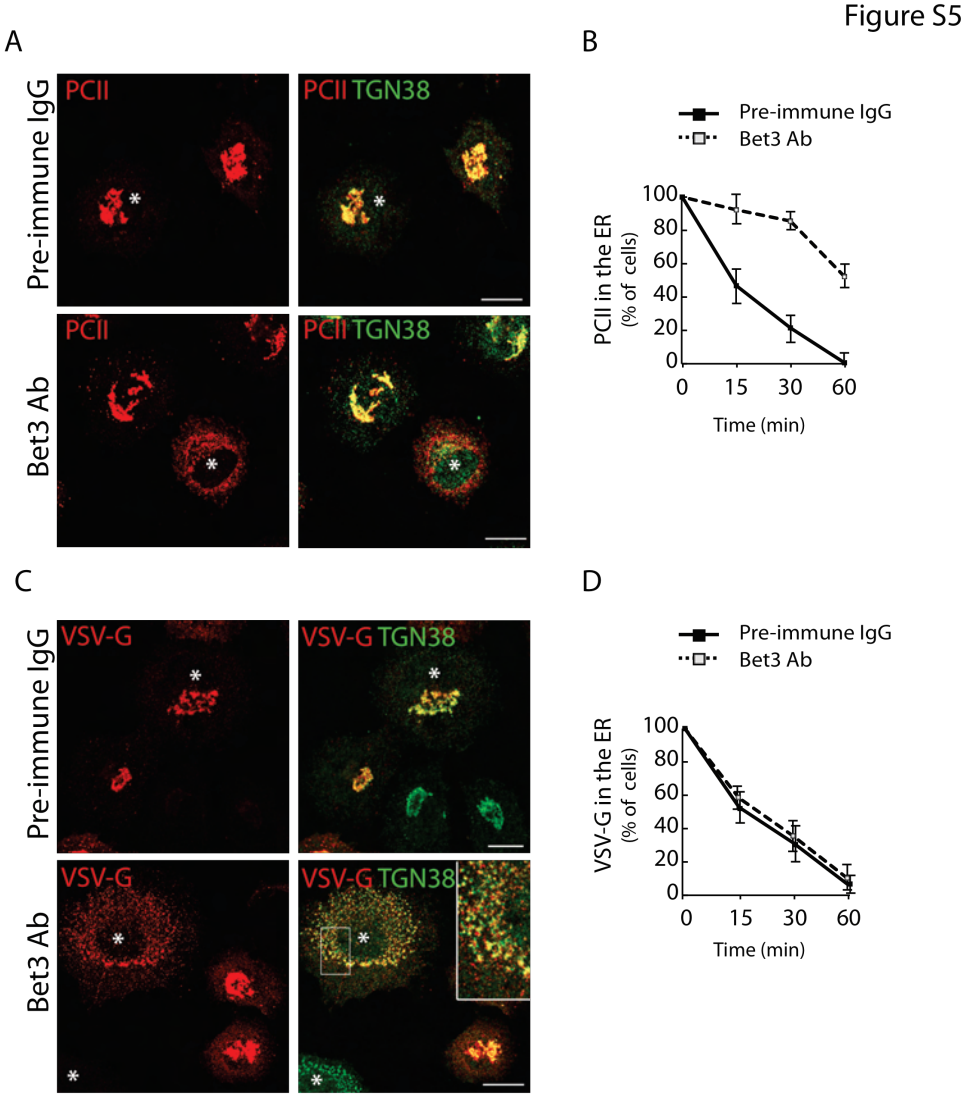

Fig. S5. The acute TRAPP block selectively impairs the ER exit of PC.
(A) Rx chondrocytes were microinjected with pre-immune IgG or an anti-Bet3 antibody (Bet3 Ab) during the 40°C block. Immunofluorescence analysis was performed 30 min after shifting to 32°C using anti-PCII and anti-TGN38 antibodies. Asterisks indicate microinjected cells. Scale bars, 10 µm. **(B)** Quantitative analysis of PCII transport in IgG- and Bet3 Ab-injected Rx chondrocytes. Cells were treated as described in (A) and analyzed at the indicated time points. The data are expressed as % cells with PCII in the ER. Mean values (± SD); N=4; n=100 cells for each time point. **(C)** VSVts045-infected Rx chondrocytes were microinjected with pre-immune IgG or an anti-Bet3 antibody (Bet3 Ab) during the 40°C block. Immunofluorescence analysis was performed 30 min after shifting to 32°C using anti-VSV-G and anti-TGN38 antibodies. Asterisks indicate microinjected cells. Inset: VSV-G is arrested in a post-ER vesicular compartment. Scale bars, 10 µm. **(D)** Quantitative analyses of VSV-G transport in IgG- and Bet3 Ab-injected Rx chondrocytes. Cells were treated as described in (C). The data are expressed as % cells with VSV-G in the ER. Mean values (± SD); N=4; n=100 cells for each time point.

A

```
sedlin WT        MSGSFYFVIVGHHDNPVFEMEFLPAGKAESKDDHRHLNQFIAHAALDLVDENMWLSNNMY
sedlin del387a   MSGSFYFVIVGHHDNPVFEMEFLPAGKAESKDDHRHLNQFIAHAALDLVDENMWLSNNMY
                 ************************************************************

sedlin WT        LKTVDKFNEWFVSAFVTAGHMRFIMLHDIRQEDGIKNFFTDVYDLYIKFSMNPFYEPNSP
sedlin del387a   LKTVDKFNEWFVSAFVTAGHMRFIMLHDIRQEDGIKNFFTDVYDLYIKFSMNPFYEPNSP
                 ************************************************************

sedlin WT        IRSSAFDRKVQFLGKKHLLS
sedlin del387a   IRSSAFDRKFSFLGRNTF--
                 *********..***:: :
```

B

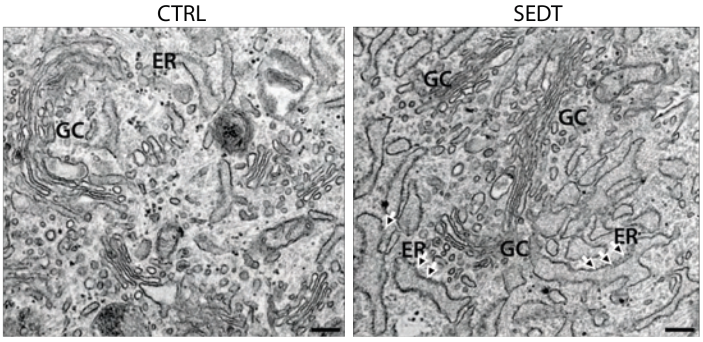

C

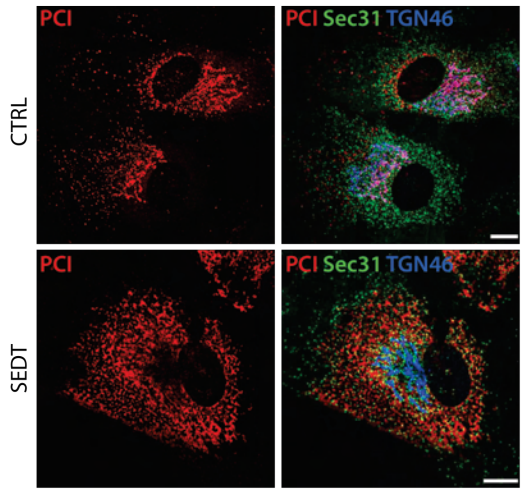

D

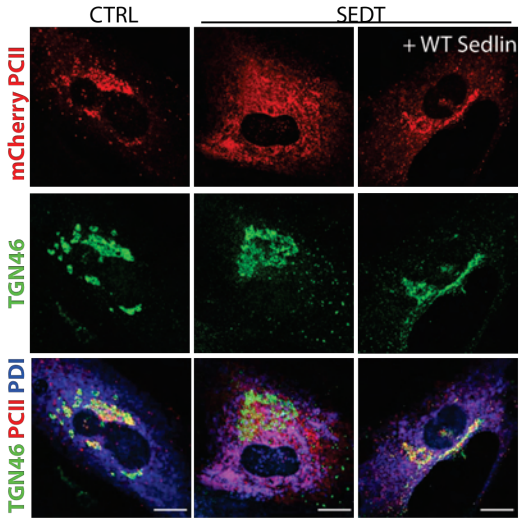

Fig. S6. Characterization of SEDT fibroblasts.
(A) Protein alignment of mutated and WT Sedlin. **(B)** Control (CTRL) and SEDT fibroblasts were processed for electron microscopy. GC, Golgi complex. Arrows indicate dilated ER. Scale bars: 200 nm. **(C)** Control (CTRL) and SEDT fibroblasts were incubated for 3 hrs at 40°C and then shifted to 32°C for 30 min. Cells were stained for PC-I (red), Sec31 (green) and TGN46 (blue). Scale bars, 10 µm. **(D)** Expression of mCherry-PCII (red) in fibroblasts from a healthy (CTRL) or SEDT subject. Where indicated, the WT Sedlin construct was co-injected with the PCII construct (+WT Sedlin). The cells were incubated at 40°C for 3 hrs, shifted to 32°C for 30 min, and processed for immunofluorescence using anti-TGN46 (a Golgi marker, green) or anti-PDI (an ER marker, blue). Scale bars, 10 µm.

Figure S7

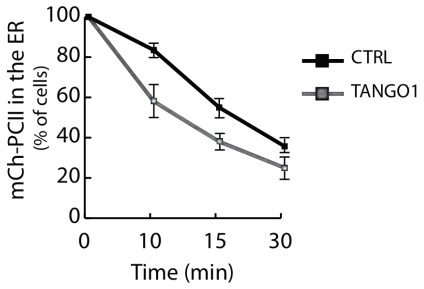

Fig. S7. Effect of TANGO1 overexpression on PCII trafficking.
HeLa cells were transfected with mCherry-PCII (CTRL) or co-transfected with mCherry-PCII and Flag-TANGO1 (TANGO1) constructs. The cells were kept at 40°C for 3 hrs and then shifted to 32°C for the indicated times. Cells were fixed and processed for immunofluorescence using anti-TGN46 (a Golgi marker) and anti-FLAG (to label Flag-TANGO1) antibodies. The transport of PCII out of the ER is expressed as % cells with PCII in the ER. Mean values (±SD); N=3, n=100 for each time point.

Figure S8

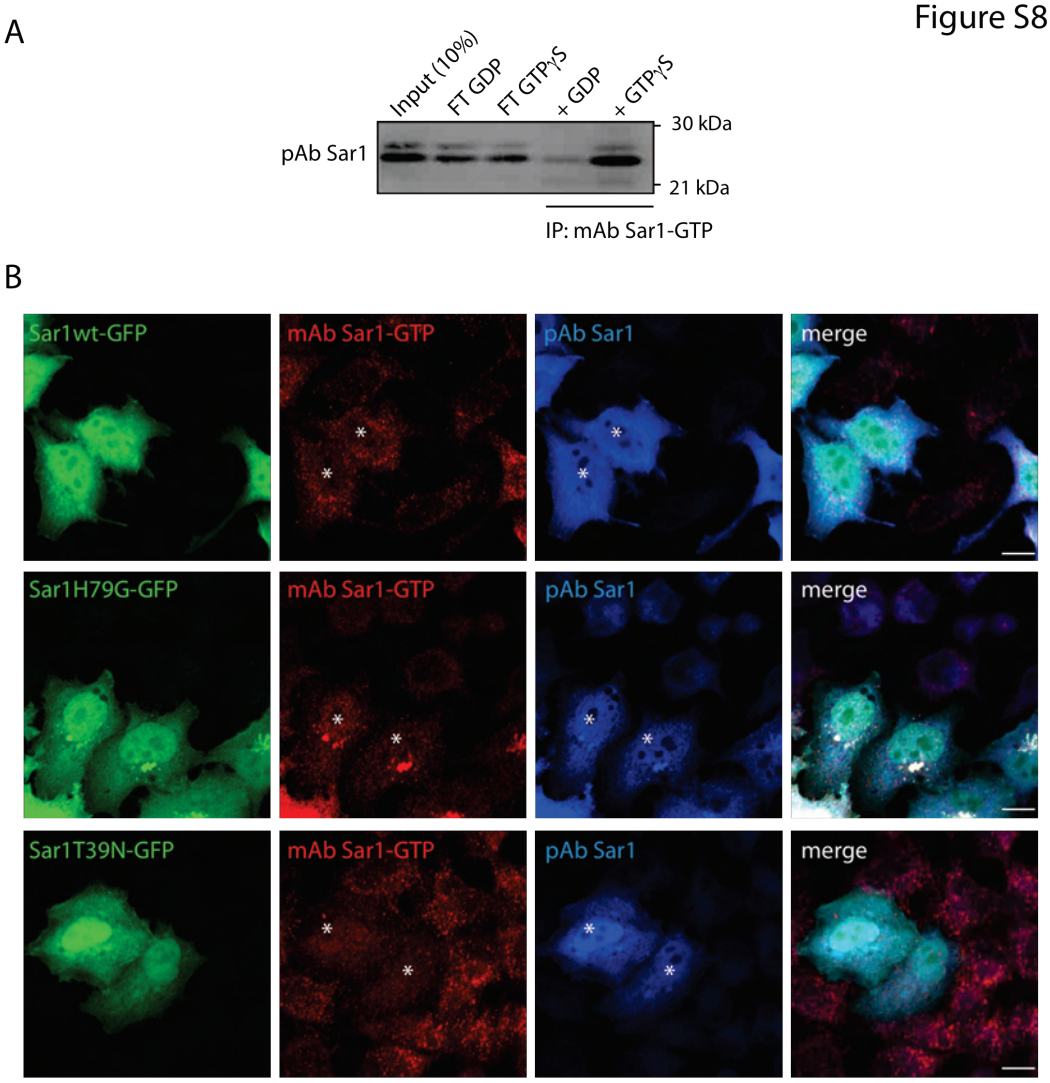

Fig. S8. Validation of the anti-active Sar1 Ab.
The specificity for Sar1-GTP of the anti-active Sar1 monoclonal Ab (NewEast Biosciences) was validated by immunoprecipitation (A) and by IF (B). **(A)** HeLa cell lysates were prepared and treated with GDP or GTPγS (see Methods) and immunoprecipitated with the anti-active Sar1 monoclonal Ab (IP: mAB Sar1-GTP); Sar1 was detected in Western Blot using the polyclonal anti-pan Sar1 Ab (pAb Sar1). Ten percent of the cell lysate was loaded as a control (Input 10%). FT: flow through. **(B)** wt Sar1, the GTP-locked constitutively-active Sar1 mutant (Sar1H79G), or the GDP-locked inactive Sar1 mutant (Sar1T39N) were expressed in HeLa cells as GFP-chimeras. The cells were stained with the anti-active Sar1 monoclonal Ab (red) and the anti-Sar1 polyclonal Ab (blue). Asterisks indicate transfected cells. Bar: 10 μm.

Figure S9

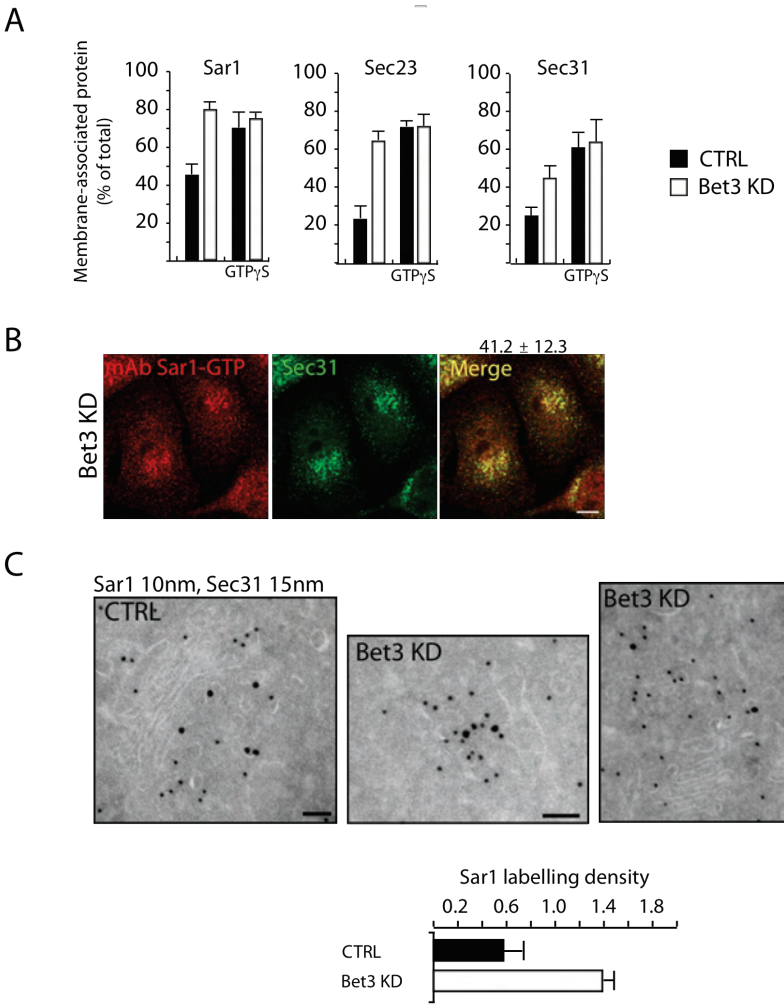

Fig. S9. TRAPP depletion stabilizes the membrane association of Sar1.
(A) HeLa cells were treated with non-targeting (CTRL) or Bet3 siRNAs for 72 hrs, then permeabilized with streptolysin O (SLO) in the absence or presence of 100 μM GTPγS (as indicated) and the supernatant and the permeabilized cells (after lysis) were analyzed by SDS-PAGE and immunoblot for the presence of Sar1, Sec23 and Sec31 as described in Fig. 3A. **(B)** Immunofluorescence of Bet3-KD cells with Sar1-GTP mAb. The cells were stained with the anti-active Sar1 monoclonal Ab (red) and the anti-Sec31 polyclonal Ab (green). The extent of co-localization of Sec31 with Sar1-GTP is indicated (41%; the co-localization in control cells is 14%, see Fig. 3B). Bar: 10 μm. **(C)** Immunoelectron microscopic analyses of HeLa cells treated with non-targeting (CTRL) and Bet3 siRNAs (Bet3 KD) show that the KD of Bet3 causes an accumulation of Sar1 on ER membranes. The graph reports the results of the quantitative analysis of Sar1 labelling density. Scale bars, 200 nm.

Figure S10

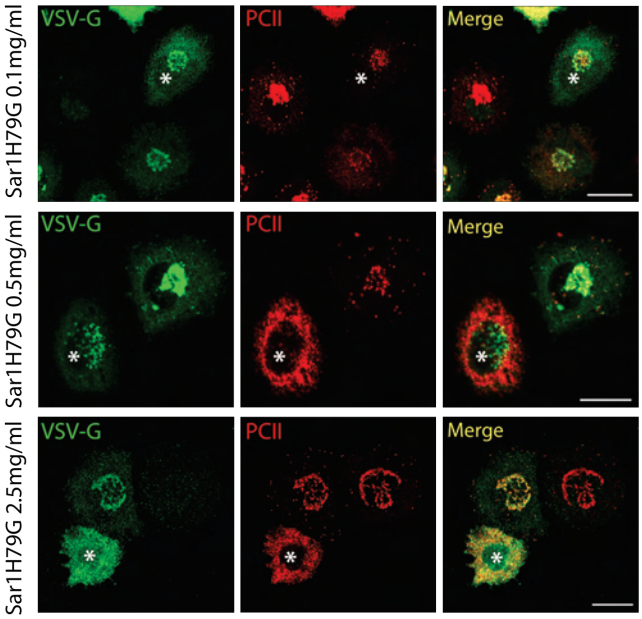

Fig. S10. The ER export of PC is impaired by Sar1-GTP levels that are permissive for VSV-G export.
Rx chondrocytes were tsO45-VSV-infected for 1 hr at 32°C and then incubated at 40°C for 3 hrs. During the last hour, cells were microinjected with Sar1H79G at the indicated dilutions and then shifted to the permissive temperature (32°C) for 30 min. VSV-G (green) and PCII (red). Asterisks indicate injected cells. Scale bars, 10μm.

Figure S11

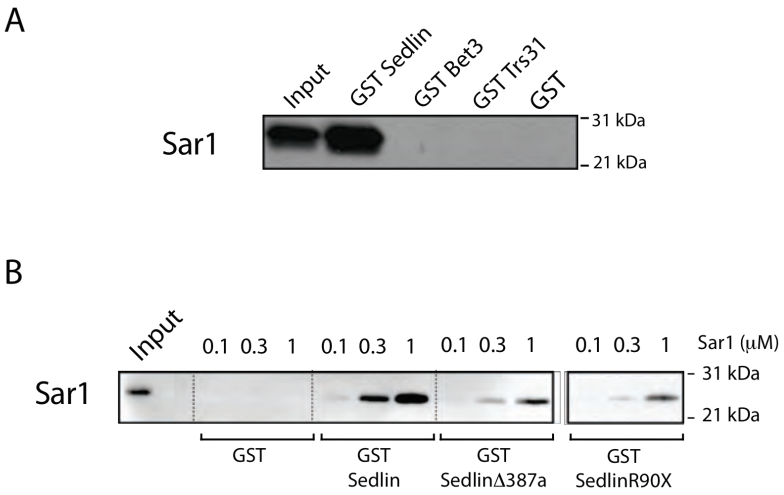

Fig. S11 Sedlin binds Sar1.
(A) Pull down of Sar1 (1 μM) with GST-tagged Sedlin, Bet3 (TRAPPC3) and Trs31 (TRAPPC5), (each 0.5 μM) or GST alone. Input 200ng Sar1. **(B)** Pull-down assays of Sar1 with GST, GST-Sedlin (Sedlin) or GST-tagged disease-associated Sedlin mutants (SedlinD387a and SedlinR90X).

Figure S12

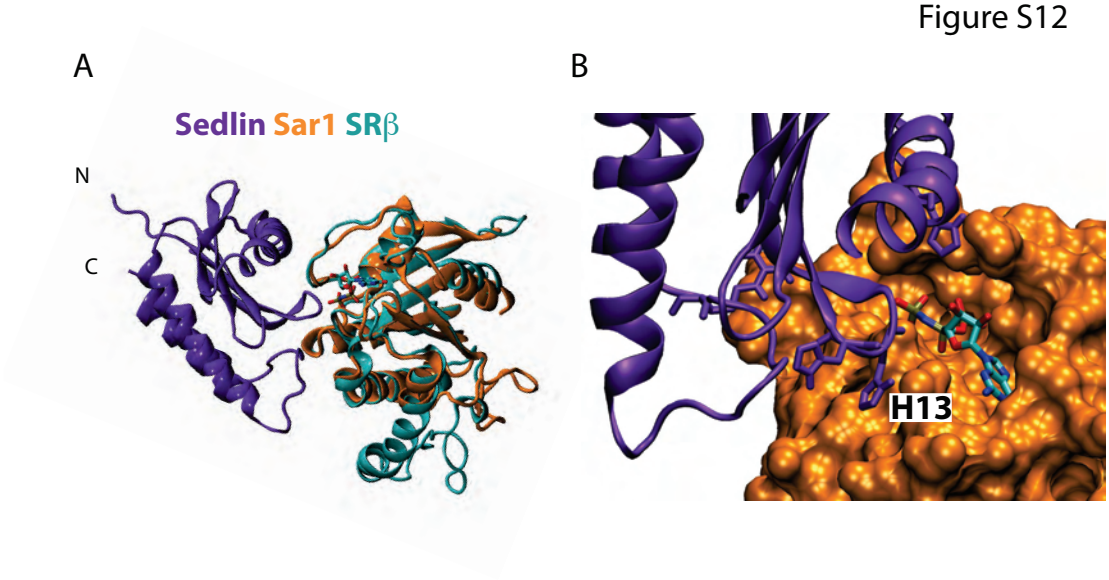

Fig. S12. Homology modeling of the Sedlin-Sar1 complex on the SRX-SRβ complex. **(A)** Sedlin has structural homology with SRX (*18*) and Sar1 was modelled on SRβ (See Materials and Methods for details). **(B)** Close up of the interaction surface between Sedlin (cyan) and Sar1 (orange) showing the involvement of the H13 residue.

Figure S13

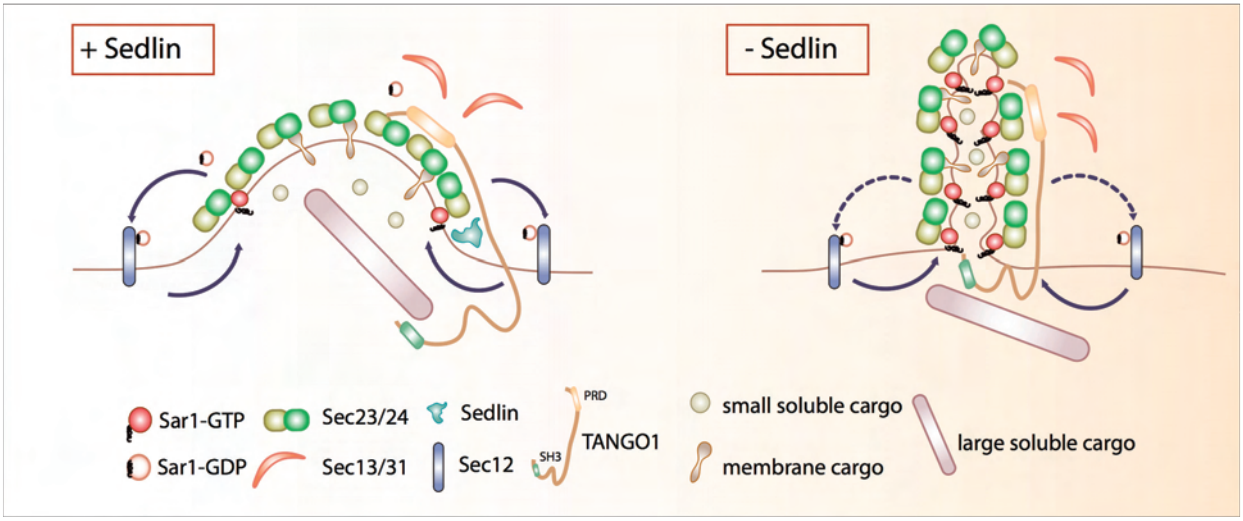

Fig. S13. Model of the role of Sedlin in the biogenesis of PC transport carriers.
Left: the activation of Sar1 by Sec12 initiates the recruitment of the COPII complex (*1*). TANGO1 assists the packaging of PC by binding PC in the ER lumen and Sec23 in the cytosol and preventing the interaction of Sec23/24 with Sec13/31 (*3*). Preventing Sec13/31 recruitment can have contrasting consequences on carrier biogenesis. On the one hand, by postponing the membrane deformation induced by Sec13/31 (*35*), it would allow the assembly of large platforms of the inner COPII layer (as required for a megacarrier) but on the other it would also slow down the Sar1 cycle and accumulate Sar1-GTP that, by inducing membrane constrictions, would antagonize the growth of megacarriers. However, TANGO1 also recruits Sedlin and Sedlin promotes Sar1 inactivation/release. Hence, the combined action of TANGO1/Sedlin coordinates the stabilization of the inner COPII layer (mediated by TANGO1) with efficient Sar1 cycling (through Sedlin) to prevent membrane constriction thus allowing the growth of the nascent carriers and the incorporation of the large PC prefibrils. **Right:** upon Sedlin depletion or mutation the Sar1 cycle is slowed down and Sar1-GTP accumulates on the nascent carrier inducing membrane constrictions. The carriers formed under these conditions are unsuited to host large cargoes, but are still able to accommodate small cargoes. Interestingly, a higher concentration of Sar1 and the presence of constricted tubular profiles at ERES have been also observed in cells from patients affected by Craniolenticulosutural dysplasia that express the F382L mutant of Sec23A that has a defective coupling with Sec31 (*36*). We propose that conditions associated with a selective impairment of PC export (36-*38* and this study) might share a deregulation of the Sar1 cycle.

Table S1

name	Sense sequence 3′-5′	Species	Purchased from
Sedl N1	GGGCAUAUGAGGUUUAUUA UU	human	Dharmacon
Sedl N2	GAGCUUCUACUUUGUAAUU UU	human	Dharmacon
Sedl N3	ACAUGUGGCUAUCGAACAA UU	human	Dharmacon
Sedl N4	CAUAAGACAAGAAGAUGGA UU	human	Dharmacon
Sedl N5	GGGCAUAUGAGAUUUAUUA UU	rat	Sigma
Sedl N6	AAGCUUCUACUUUGUAAUU UU	rat	Sigma
Sedl N7	AUAUGUGGCUUUCUAACAA UU	rat	Sigma
Sedl N8	UGUGAGGCAAGAAGAUGGA UU	rat	Sigma
Sedl S1	UCCAUUUUAUGAACCCAAU UU	human/rat	Sigma
Sedl S2	CAAUUCUCCUAUUCGAUCA UU	human/rat	Sigma
Bet3 N1	GAUAACCACUCAUCCCUUA UU	human	Dharmacon
Bet3 N2	GGGCAUCACUCCAAGCAUU UU	human/rat	Dharmacon
Bet3 N3	GAAAGGAGACGGUGUGACA UU	human	Dharmacon
Bet3 N4	GGAAACUGCGGAUGUCAUU UU	human	Dharmacon
TANGO1 N1	GCAAUAACCUCAACUCUAU UU	human	Sigma
TANGO1 N2	GCAAGAAACUAGUAUGAUU UU	human	Sigma
TANGO1 N3	GAACUGUCCUUGUUGUGAA UU	human	Sigma
TANGO1 N4	GAUAAGGUCUUCCGUGCUU UU	human	Sigma

Table S1.

Sequences of siRNA oligos used in this study.

References

1. G. Zanetti, K. B. Pahuja, S. Studer, S. Shim, R. Schekman, COPII and the regulation of protein sorting in mammals. *Nat. Cell Biol.* **14**, 20 (2012). doi:10.1038/ncb2390

2. K. Saito *et al*., TANGO1 facilitates cargo loading at endoplasmic reticulum exit sites. *Cell* **136**, 891 (2009). doi:10.1016/j.cell.2008.12.025 Medline

3. V. Malhotra, P. Erlmann, Protein export at the ER: Loading big collagens into COPII carriers. *EMBO J.* **30**, 3475 (2011). doi:10.1038/emboj.2011.255 Medline

4. D. G. Wilson *et al*., Global defects in collagen secretion in a Mia3/TANGO1 knockout mouse. *J. Cell Biol.* **193**, 935 (2011). doi:10.1083/jcb.201007162 Medline

5. A. K. Gedeon *et al*., Identification of the gene (SEDL) causing X-linked spondyloepiphyseal dysplasia tarda. *Nat. Genet.* **22**, 400 (1999). doi:10.1038/11976 Medline

6. G. E. Tiller *et al*., A recurrent RNA-splicing mutation in the SEDL gene causes X-linked spondyloepiphyseal dysplasia tarda. *Am. J. Hum. Genet.* **68**, 1398 (2001). doi:10.1086/320594 Medline

7. J. Barrowman, D. Bhandari, K. Reinisch, S. Ferro-Novick, TRAPP complexes in membrane traffic: Convergence through a common Rab. *Nat. Rev. Mol. Cell Biol.* **11**, 759 (2010). doi:10.1038/nrm2999 Medline

8. J. F. Bleasel *et al*., Type II procollagen gene (COL2A1) mutation in exon 11 associated with spondyloepiphyseal dysplasia, tall stature and precocious osteoarthritis. *J. Rheumatol.* **22**, 255 (1995). Medline

9. A. Zankl *et al*., Spondyloperipheral dysplasia is caused by truncating mutations in the C-propeptide of COL2A1. *Am. J. Med. Genet. A* **129A**, 144 (2004). doi:10.1002/ajmg.a.30222 Medline

10. See supplementary materials on *Science* Online.

11. A. A. Mironov *et al*., Small cargo proteins and large aggregates can traverse the Golgi by a common mechanism without leaving the lumen of cisternae. *J. Cell Biol.* **155**, 1225 (2001). doi:10.1083/jcb.200108073 Medline

12. P. J. Scrivens *et al*., TRAPPC2L is a novel, highly conserved TRAPP-interacting protein. *Traffic* **10**, 724 (2009). doi:10.1111/j.1600-0854.2009.00906.x Medline

13. R. Pepperkok, M. Lowe, B. Burke, T. E. Kreis, Three distinct steps in transport of vesicular stomatitis virus glycoprotein from the ER to the cell surface in vivo with differential sensitivities to GTPγS. *J. Cell Sci.* **111**, 1877 (1998). Medline

14. K. R. Long *et al*., Sar1 assembly regulates membrane constriction and ER export. *J. Cell Biol.* **190**, 115 (2010). doi:10.1083/jcb.201004132 Medline

15. K. Bacia *et al*., Multibudded tubules formed by COPII on artificial liposomes. *Sci. Rep.* **1**, 17 (2011). doi:10.1038/srep00017 Medline

16. X. Bi, R. A. Corpina, J. Goldberg, Structure of the Sec23/24-Sar1 pre-budding complex of the COPII vesicle coat. *Nature* **419**, 271 (2002). doi:10.1038/nature01040 Medline

17. S. B. Jang *et al*., Crystal structure of SEDL and its implications for a genetic disease spondyloepiphyseal dysplasia tarda. *J. Biol. Chem.* **277**, 49863 (2002). doi:10.1074/jbc.M207436200 Medline

18. O. Schlenker, A. Hendricks, I. Sinning, K. Wild, The structure of the mammalian signal recognition particle (SRP) receptor as prototype for the interaction of small GTPases with Longin domains. *J. Biol. Chem.* **281**, 8898 (2006). doi:10.1074/jbc.M512415200 Medline

19. H. Cai *et al*., TRAPPI tethers COPII vesicles by binding the coat subunit Sec23. *Nature* **445**, 941 (2007). doi:10.1038/nature05527 Medline

20. C. Lord *et al*., Sequential interactions with Sec23 control the direction of vesicle traffic. *Nature* **473**, 181 (2011). doi:10.1038/nature09969 Medline

21. P. Marra *et al*., The biogenesis of the Golgi ribbon: The roles of membrane input from the ER and of GM130. *Mol. Biol. Cell* **18**, 1595 (2007). doi:10.1091/mbc.E06-10-0886 Medline

22. G. D'Angelo *et al*., GRASP65 and GRASP55 sequentially promote the transport of C-terminal valine-bearing cargos to and through the Golgi complex. *J. Biol. Chem.* **284**, 34849 (2009). doi:10.1074/jbc.M109.068403 Medline

23. K. B. King, J. H. Kimura, The establishment and characterization of an immortal cell line with a stable chondrocytic phenotype. *J. Cell. Biochem.* **89**, 992 (2003). doi:10.1002/jcb.10571 Medline

24. J. Gécz *et al*., Gene structure and expression study of the SEDL gene for spondyloepiphyseal dysplasia tarda. *Genomics* **69**, 242 (2000). doi:10.1006/geno.2000.6326 Medline

25. L. Poliseno *et al*., A coding-independent function of gene and pseudogene mRNAs regulates tumour biology. *Nature* **465**, 1033 (2010). doi:10.1038/nature09144 Medline

26. S. Yu *et al*., mBet3p is required for homotypic COPII vesicle tethering in mammalian cells. *J. Cell Biol.* **174**, 359 (2006). doi:10.1083/jcb.200603044 Medline

27. H. F. Lodish, N. Kong, Glucose removal from N-linked oligosaccharides is required for efficient maturation of certain secretory glycoproteins from the rough endoplasmic reticulum to the Golgi complex. *J. Cell Biol.* **98**, 1720 (1984). doi:10.1083/jcb.98.5.1720 Medline

28. P. Watson, R. Forster, K. J. Palmer, R. Pepperkok, D. J. Stephens, Coupling of ER exit to microtubules through direct interaction of COPII with dynactin. *Nat. Cell Biol.* **7**, 48 (2005). doi:10.1038/ncb1206 Medline

29. H. Hughes *et al*., Organisation of human ER-exit sites: Requirements for the localisation of Sec16 to transitional ER. *J. Cell Sci.* **122**, 2924 (2009). doi:10.1242/jcs.044032 Medline

30. E. L. Snapp, N. Altan, J. Lippincott-Schwartz, *Curr. Protoc. Cell Biol*., chapter 21, unit 21.1 (2003).

31. M. A. De Matteis, G. Santini, R. A. Kahn, G. Di Tullio, A. Luini, Receptor and protein kinase C-mediated regulation of ARF binding to the Golgi complex. *Nature* **364**, 818 (1993). doi:10.1038/364818a0 Medline

32. T. Daniele, G. Di Tullio, M. Santoro, G. Turacchio, M. A. De Matteis, ARAP1 regulates EGF receptor trafficking and signalling. *Traffic* **9**, 2221 (2008). doi:10.1111/j.1600-0854.2008.00823.x Medline

33. F. Kiefer, K. Arnold, M. Künzli, L. Bordoli, T. Schwede, The SWISS-MODEL Repository and associated resources. *Nucleic Acids Res.* **37**, D387 (2009). doi:10.1093/nar/gkn750 Medline

34. Y. G. Kim *et al*., The architecture of the multisubunit TRAPP I complex suggests a model for vesicle tethering. *Cell* **127**, 817 (2006). doi:10.1016/j.cell.2006.09.029 Medline

35. S. M. Stagg *et al*., Structural basis for cargo regulation of COPII coat assembly. *Cell* **134**, 474 (2008). doi:10.1016/j.cell.2008.06.024 Medline

36. J. C. Fromme *et al*., The genetic basis of a craniofacial disease provides insight into COPII coat assembly. *Dev. Cell* **13**, 623 (2007). doi:10.1016/j.devcel.2007.10.005 Medline

37. A. K. Townley *et al*., Efficient coupling of Sec23-Sec24 to Sec13-Sec31 drives COPII-dependent collagen secretion and is essential for normal craniofacial development. *J. Cell Sci.* **121**, 3025 (2008). doi:10.1242/jcs.031070 Medline

38. S. A. Boyadjiev *et al*., Cranio-lenticulo-sutural dysplasia associated with defects in collagen secretion. *Clin. Genet.* **80**, 169 (2011). doi:10.1111/j.1399-0004.2010.01550.x Medline